Applied Physics Express

LETTER

Thermal characterization of electrically injected GaN-based microdisk lasers on Si

Applied Physics Express 13, 074002 (2020) LETTER
https://doi.org/10.35848/1882-0786/ab95f0

Thermal characterization of electrically injected GaN-based microdisk lasers on Si

Jin Wang[1,2], Meixin Feng[2,3*], Rui Zhou[2,3], Qian Sun[2,3,4*], Jianxun Liu[2], Xiujian Sun[2], Xinhe Zheng[1*], Xing Sheng[5], and Hui Yang[2,4]

[1]University of Science and Technology Beijing, Beijing 100083, People's Republic of China
[2]Key Laboratory of Nano-devices and Applications, Suzhou Institute of Nano-Tech and Nano-Bionics, Chinese Academy of Sciences (CAS), Suzhou 215123, People's Republic of China
[3]Suzhou Institute of Nano-Tech and Nano-Bionics, CAS, Foshan 528000, People's Republic of China
[4]School of Nano Technology and Nano Bionics, University of Science and Technology of China, Hefei, 230026, People's Republic of China
[5]Department of Electronic Engineering, Tsinghua University, Beijing, 100084, People's Republic of China

*E-mail: mxfeng2011@sinano.ac.cn; qsun2011@sinano.ac.cn; xinhezheng@ustb.edu.cn

Received March 11, 2020; revised May 20, 2020; accepted May 22, 2020; published online June 4, 2020

GaN-based microdisk lasers grown on Si have a wide application prospect in communication and Si photonics. However, the relatively large threshold current and thermal resistance often cause a very high junction temperature, which severely affects the device performance. Here we analyzed the thermal characteristics of GaN-based microdisk lasers grown on Si substrates. According to the simulation results, we have significantly reduced the threshold current and junction temperature by reducing the current injection area and device size, respectively. As a result, continuous wave electrically injected lasing has been achieved at room temperature for both microring and microdisk lasers grown on Si.

Supplementary material for this article is available online

Microcavity lasers featured with low-loss whispering gallery modes have been drawing increasing attention in communication, biological detection, temperature sensors and some other fields, due to their particular advantages of a small footprint, low power consumption and high quality factor compared with conventional laser diodes with Fabry–Pérot cavity.[1–4] GaN-based microdisk laser grown on Si is one of the promising candidates for the on-chip light source of the optical interconnection,[5–7] because of the compatibility with Si-based microelectronics and low-cost large-scale manufacturing foundry.[8–11]

In our previous work, we adopted a "sandwich-like" architecture by using AlGaN cladding layers on both sides of quantum wells for better electrical conductivity and reduced thermal resistance (R_{th}) than the conventional "mushroom-like" structure, and realized the first electrically pumped GaN-on-Si microdisk laser, of which the lasing wavelength and threshold current were 412 nm (violet) and 250 mA, respectively.[12] We also achieved the demonstration of electrically injected GaN-based ultraviolet (386 nm) microdisk laser diodes by overcoming the challenge of epitaxial growth and defects, and the threshold current was 248 mA.[13] However, the device above can only operate in a pulsed mode, because of the high junction temperature induced by the relatively high threshold current and threshold voltage. High junction temperature will increase the nonradiative recombination of the active region[14–17] and accelerate the diffusion of defects along threading dislocations,[18–20] which are detrimental to the internal quantum efficiency. Meanwhile, elevated junction temperature can increase the kinetic energy of electrons, and weaken the carrier confinement, thus reducing the injection efficiency. In addition, high junction temperature can also cause newly generated defects of cavity facets, affecting the reliability of the laser device.[21,22] These negative effects will form a feedback and increase the junction temperature further, and hence deteriorate the laser performance.[23,24] Therefore, it is necessary to analyze the thermal characteristics of the microdisk laser and reduce the junction temperature to improve the device performance.[25,26]

Based on our previous work of the violet microdisk laser reported in Feng et al.,[12] we first reduced the carbon concentration in p-AlGaN cladding layer as reported in Liu et al.[27] After that, the threshold current density and threshold voltage of the device with an outer and inner radii of 20 and 10 μm (abbreviated as 20–10 μm microring) were reduced down to 8 kA cm^{-2} and 6 V, respectively. However, it still cannot operate in a continuous wave (CW) mode because of the high junction temperature at the threshold. Therefore, in this work, we analyzed the thermal characteristics of violet microdisk lasers to reduce the junction temperature at threshold by changing the device structure. According to the simulation results, we have significantly reduced the threshold current and junction temperature by reducing the current injection area and device size, respectively. As a result, CW electrically injected lasing has been achieved at room temperature for both microring and microdisk lasers grown on Si.

In this work, the thermal characteristics of GaN-based microdisk laser were analyzed by the finite element method and we assume all the heat dissipates through the heat sink at the bottom of the laser device, and the heat transfer with air can be neglected because of the small thermal conductivity (TC) of air. The heat dissipation process follows the heat equation,

$$\nabla(-k\nabla T) = Q$$

$$k\nabla T = h(T_{inf} - T)$$

where k, T, Q, h, T_{inf} are the TC, temperature, heat source density, heat transfer coefficient, and heat sink temperature, respectively. For GaN-based microdisk lasers, the relatively low optical power could be ignored compared with the injected electrical power at the threshold current, and it is reasonable to assume that all the injected electrical power is converted into heat. According to the literature,[28] the injected electrical power converts into heat in two major ways, the nonradiative recombination from the active region and the joule heat from the p-type layers with a relatively high resistance. Therefore, the heat source was set at the

active region and p-type layers, and the Q at threshold could be defined as

$$Q = \frac{U_{th} \cdot I_{th}}{V}$$

where U_{th} and I_{th} are threshold voltage and threshold current, respectively. V is the volume of the active region and p-type layers, which vary with the size of the device. As reported in Campenhout et al.,[26] the threshold current density and the threshold voltage did not change with the radius of the microdisk lasers. Therefore, in this simulation, we assumed all the devices with the same threshold current density (8 kA cm^{-2}) and threshold voltage (6 V). The detailed parameters of the thickness and TC for each layer are shown in Table I.[29,30]

Figure 1 shows the simulation results of the microring lasers, of which the outer circle radius was 20 μm and the inner radius varied from 0 to 15 μm. The microring structure is shown in Fig. 1(a). The inner circle was etched to p-AlGaN cladding layer and covered by the SiO_2 insulation layer, the current is injected only from the ring area, and recombination occurs in the active region underneath the ring area. Therefore, the heat source was set at the ring area of THE p-type layer and active region.

As shown in Fig. 1(b), the fluctuation of thermal resistance was relatively small, about only 30 K W^{-1}. The reason is that the pathway of downward heat dissipation is basically the same for the devices with the same outer radius. A brief qualitative explanation of thermal resistance is as following. When the inner circle is small, the center region without heat generation is so small that it will not make the heat density of the annular region increase too much, but it will provide an effective cooling channel, resulting in a slightly lower thermal resistance. When the inner circle is too large, the cooling channel effect is saturated because of the limited ability of lateral heat dissipation, but the larger inner circle leads to less area of annular region, which means a higher heat density and less heat dissipating area through the substrate, causing a higher thermal resistance. The simulation results of thermal resistance were consistent with the test results. For more details, see the supplementary data, available online at stacks.iop.org/APEX/13/074002/mmedia.

Combining with the threshold current and threshold voltage, the temperature rise at threshold current decreased from 88 to 40 K with the radius of inner circle increased from 0 to 15 μm. For the 20–0 μm microring laser, the temperature rise at threshold current was estimated to be 88 K, as shown in Fig. 1(c). As for the 20–5 μm microring laser, because of the reduced current injection area, the threshold current and also the injected electrical power were decreased. Meanwhile, the inner circle provides an extra heat dissipating channel. Therefore, the temperature rise at threshold was reduced to 71 K, as shown in Fig. 1(d). For the case of 20–10 μm and 20–15 μm microring lasers, though the cooling channel effect was gradually saturated, the significant reduction of threshold current and power consumption dominated in this case, as shown in Fig. 1(e). Consequently, the temperature rise at threshold of 20–10 μm and 20–15 μm microring lasers were 58 and 40 K, respectively. Therefore, an effective way to realize CW lasing of microdisk lasers is to increase the size of the inner circle.

After the fabrication of the devices, we measured the electroluminescence (EL) power-current (P–I) curves under pulsed current injection with various duty cycles. Figure 2(a) shows that the knee point in the P–I curve was disappeared, and the output power was largely dropped at high current level when the duty cycle was increased from 8% to 64%. However, for the 20–15 μm microring laser, when the duty cycle was increased from 4% to 100%, the device could still lase, and the threshold current was only increased a little due to the effective reduction of the junction temperature. The EL spectra of the 20–15 μm microring laser under various CW currents are shown in Fig. 2(c). There was a spontaneous emission broad peak around 410 nm under a small current injection. When the current was above the threshold (50 mA), a sharp lasing emission peak at 411 nm was observed, and the full width at half maximum (FWHM) of the spectrum was narrowed down to 0.5 nm, as shown in the blue line of Fig. 2(d). The characteristics indicate a room temperature CW electrically pumped lasing of the GaN-based 20–15 μm microring lasers grown on Si.

In addition to the applied microring structure, another effective way to realize CW electrically injected lasing is to shrink the device size. Usually, a microdisk laser device with

Table I. The material parameters used in the simulation.

Layer	Material	Thickness (nm)	TC ($W \cdot mK^{-1}$)
Metal	Ti/Pt/Au	650	200
p-Contact 2	InGaN	5	40
p-Contact 1	GaN	30	130
p-Cladding	$Al_{0.2}Ga_{0.8}N$/GaN	600	96
Electron blocking layer	$Al_{0.18}Ga_{0.82}N$	20	30
p-Waveguide 1	GaN	20	130
p-Waveguide 2	$In_{0.01}Ga_{0.99}N$/GaN	70	105
Active region	$In_{0.12}Ga_{0.88}N/In_{0.02}Ga_{0.98}N$	52	56
n-Waveguide 2	$In_{0.01}Ga_{0.99}N$/GaN	80	105
n-Waveguide 1	GaN	40	130
n-Cladding	$Al_{0.085}Ga_{0.915}N$/GaN	1200	60
n-Contact	GaN	1300	130
Buffer 2	$Al_{0.17}Ga_{0.83}N$	310	30
Buffer 1	$Al_{0.35}Ga_{0.65}N$	180	20
Nucleation layer	AlN	280	170
Substrate	Si	10^5	145
Heat sink	Cu	10^6	400

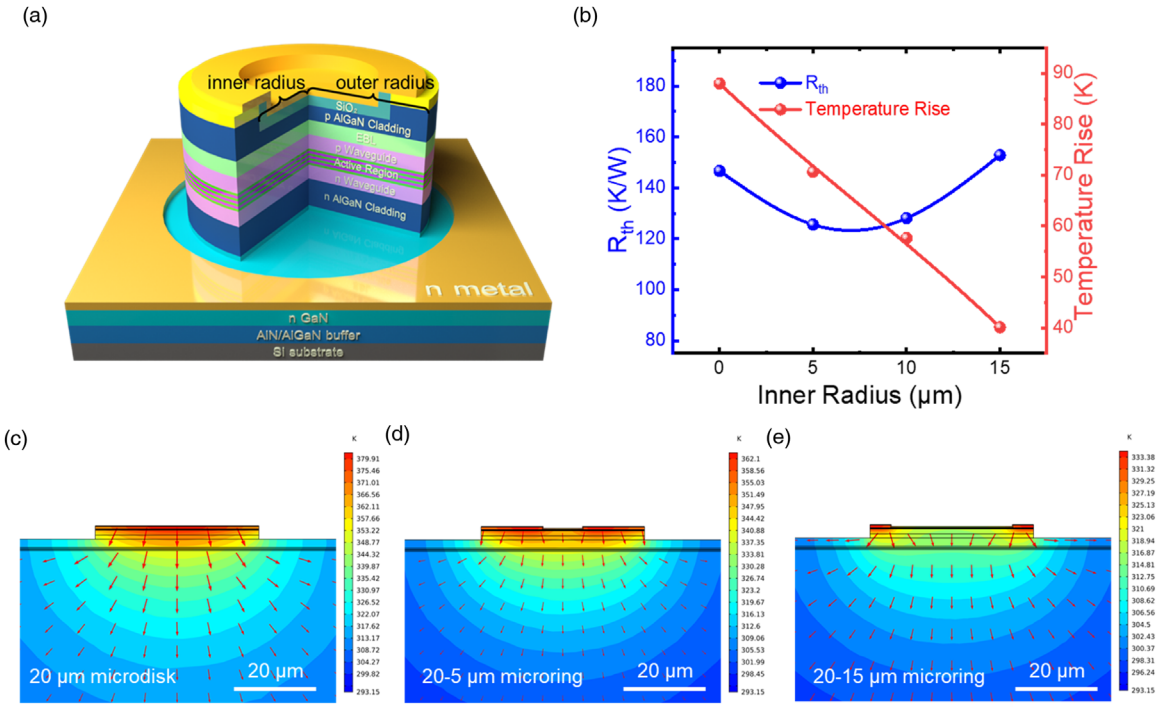

Fig. 1. (Color online) (a) Schematic illustrations of the microring laser. (b) Thermal resistance and temperature rise at threshold of microring lasers as a function of inner radius. Isotherm surface distribution and heat flux at a threshold of (c) 20–0 μm, (d) 20–5 μm and (e) 20–15 μm microring lasers.

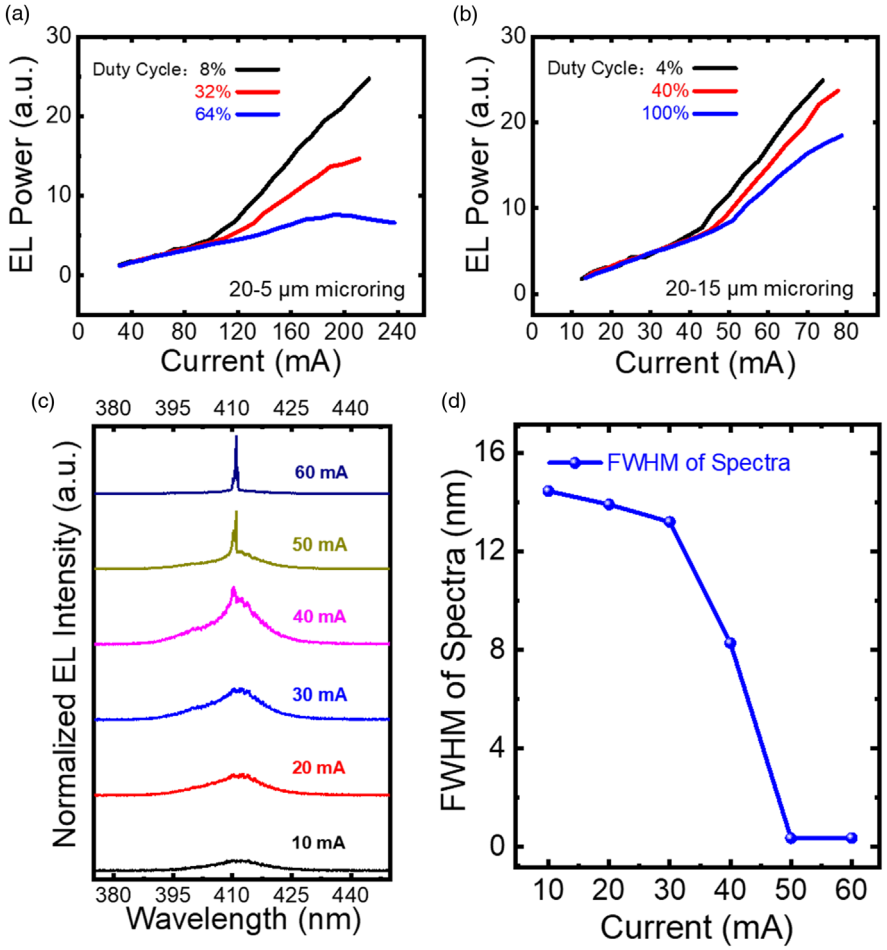

Fig. 2. (Color online) The *P–I* curves of (a) 20–5 μm and (b) 20–15 μm microring lasers under various duty cycles. (c) The EL spectra of the 20–15 μm microring laser measured under various CW currents. (d) The FWHM of spectra as a function of the injected current.

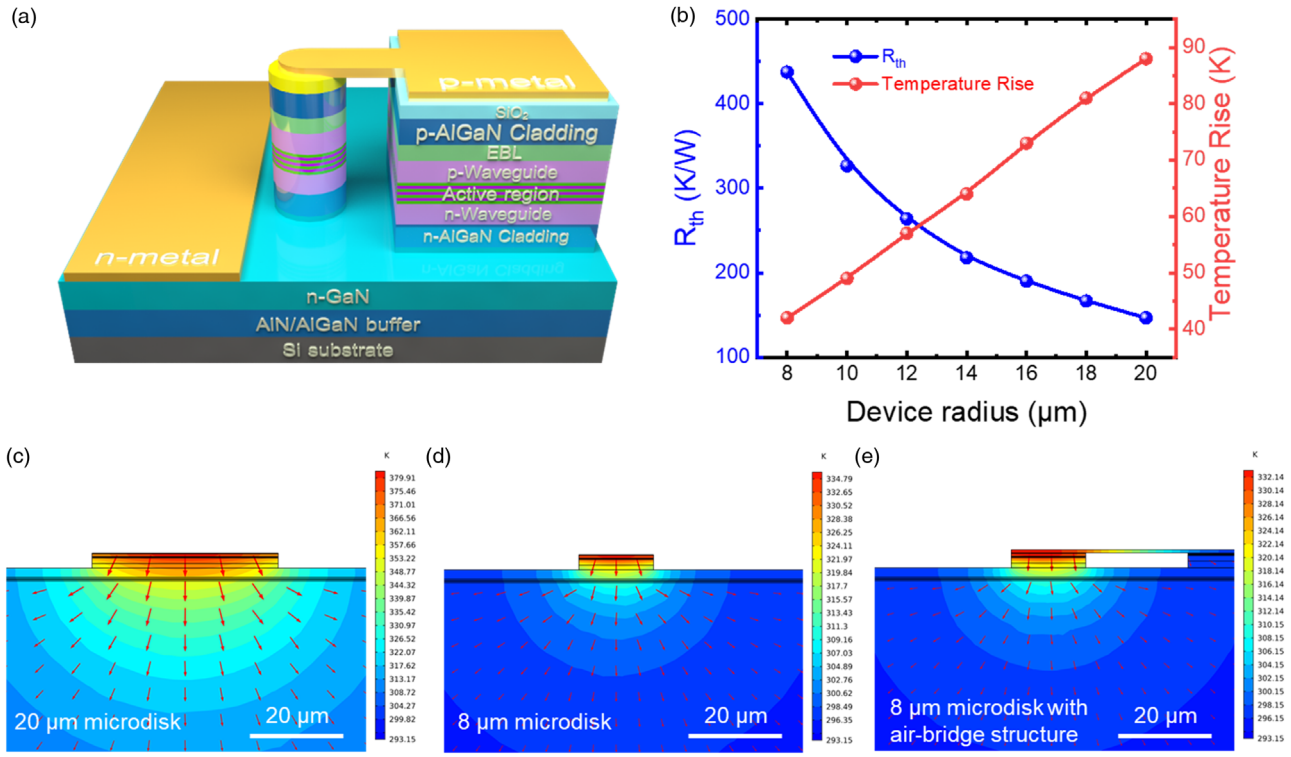

Fig. 3. (Color online) (a) Schematic illustrations of the microdisk laser with an air-bridge structure. (b) R_{th} and temperature rise of microdisk lasers at threshold as a function of device radius. Isotherm surface distribution and heat flux at threshold of microdisk laser with a radius of (c) 20 μm, (d) 8 μm and (e) 8 μm with air-bridge structure.

a smaller radius has a lower threshold current and power consumption, and is more likely to work in a CW mode. Therefore, the thermal characteristics of microdisk lasers with various radii were analyzed. In the actual device structure, for the electrical testing of microdisk laser device with a radius of less than 20 μm, the p-pad is too small to inject current by using a regular probe pin. Therefore, the air-bridge electrode structure connecting the p-type contact with a large square metal pad was designed for the convenience of device testing, as shown in Fig. 3(a), so the effect of air-bridge was also analyzed. Figure 3(b) shows the thermal resistance and temperature rise at the threshold as a function of the device radius. The thermal resistance increases from 146 to 437 K W^{-1} with the radius of device decreasing from 20 to 8 μm. From the isotherm surface distribution and heat flux marked by the arrows in Figs. 3(c) and 3(d), the heat dissipates through the substrate and heat sink underneath the device, a larger device size means a wider heat-dissipating path and a higher cooling efficiency. Therefore, small devices give a high thermal resistance. Additionally, the thermal resistance of the microdisk laser with the air-bridge structure showed a 5% reduction compared with the device of the same size without air-bridge, indicating an effect of supplemental heat dissipation through the air-bridge structure, as the comparison of Figs. 3(d) and 3(e).

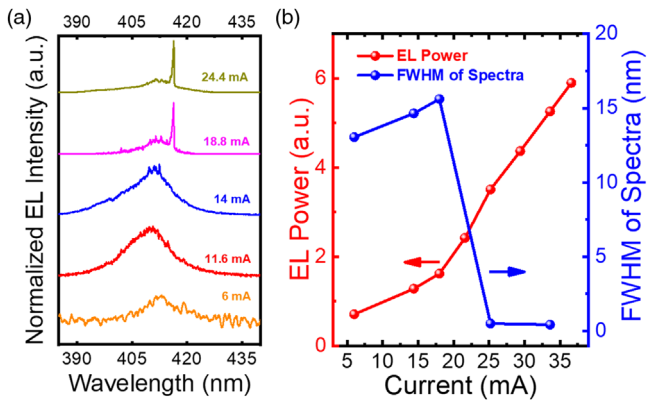

Fig. 4. (Color online) (a) The EL spectra of the microdisk laser measured under various CW currents. (b) The EL power and FWHM of spectra as a function of the injected current.

Though the thermal resistance of the small microdisk laser was high, the temperature rise at threshold was relatively low because of the great reduction in power consumption at threshold. The temperature rise of the device with a radius of 8 μm was only 42 K, while it was 88 K for the device with a radius of 20 μm, as shown in Figs. 3(c) and 3(d). As a result, we demonstrated another room-temperature CW electrically injected GaN-based microdisk lasers with a radius of 8 μm. The characteristics are shown in Fig. 4. The threshold current and lasing wavelength were 18 mA and 415 nm, respectively.

The CW operation lifetime of the as-fabricated microdisk and microring lasers mentioned above, measured at 1.1 times of the threshold current under CW injection, was estimated to be about a few minutes before a dramatic decay of output power. Further improvement of lifetime can be obtained by combining the two methods, applying microring structure for the device with a small radius, which requires a more advanced fabrication process for patterning.

In summary, the thermal characteristics of microdisk and microring lasers were studied by simulation and experiment. For microring lasers, the thermal resistance shows a relatively small fluctuation range with the inner circle ranging from 0 to 15 μm, while the junction temperature rise at threshold monotonically decreases. For microdisk lasers, the thermal

resistance increases, while the junction temperature rise at threshold decreases with the radius of microdisk lasers reducing from 20 to 8 μm. Based on the simulation result and analyses, room-temperature CW electrically injected lasing has been achieved for both microring and microdisk lasers grown on Si.

Acknowledgments The authors are grateful for the financial support from the Key-Area Research and Development Program of GuangDong Province (Grant No. 2019B010130001, 2019B090917005 and 2020B010174004), the National Key R&D Program (Grant Nos. 2016YFB0400100, 2016YFB0400104, 2018YFA0703702), the National Natural Science Foundation of China (Grant Nos. 61534007, 61775230, 61804162, and 61874131), the Strategic Priority Research Program of CAS (Grant No. XDB43000000, XDB43020200), the Key Research Program of Frontier Sciences, CAS (Grant Nos. QYZDB-SSW-JSC014, and ZDBS-LY-JSC040), the CAS Interdisciplinary Innovation Team, the Key R&D Program of Jiangsu Province (Grant No. BE2017079), the Natural Science Foundation of Jiangsu Province (Grant No. BK20180253), the Natural Science Foundation of Jiangxi Province (Grant No. 20181ACB20002), the Suzhou Science and Technology Program (Grant Nos. SYG201846, and SYG201927), and the China Postdoctoral Science Foundation (Grant No. 2018M632408). This work was also supported by the Open Fund of the State Key Laboratory of Reliability and Intelligence of Electrical Equipment (Grant No. EERIKF2018001). We are thankful for the technical support from the Nano Fabrication Facility, Platform for Characterization & Test, and Nano-X of SINANO, CAS.

ORCID iDs Jianxun Liu https://orcid.org/0000-0001-8485-166X

1) K. J. Vahala, Nature **424**, 839 (2003).
2) A. C. Tamboli, E. D. Haberer, R. Sharma, K. Lee, S. Nakamura, and E. L. Hu, Nat. Photonics **1**, 61 (2007).
3) Y. Wan et al., Optica **4**, 940 (2017).
4) J. Sellés et al., Appl. Phys. Lett. **109**, 231101 (2016).
5) F. Tabataba-Vakili et al., ACS Photonics **5**, 3643 (2018).
6) F. Tabataba-Vakili et al., Sci. Rep. **9**, 18095 (2019).
7) Y. C. Yang, B. C. Zhu, Z. Shi, J. Y. Wang, X. Li, X. M. Gao, J. L. Yuan, Y. H. Li, Y. Jiang, and Y. J. Wang, Opt. Mater. **66**, 659 (2017).
8) Y. Sun et al., Nat. Photonics **10**, 595 (2016).
9) Y. Sun et al., Light: Sci. Appl. **7**, 13 (2018).
10) M. X. Feng et al., ACS Photon **5**, 699 (2018).
11) M. X. Feng et al., IEEE J. Sel. Top. Quantum Electron. **24**, 8200305 (2018).
12) M. Feng et al., Opt. Express **26**, 5043 (2018).
13) J. Wang et al., Photonics Res. **7**, B32 (2019).
14) D. Sizov, R. Bhat, J. Wang, and C. E. Zah, Appl. Phys. Express **7**, 112701 (2014).
15) O. Pursiainen, N. Linder, A. Jaeger, R. Oberschmic, and K. Streubel, Appl. Phys. Lett. **79**, 2895 (2001).
16) J. Muller, G. Bruderl, M. Schillgalies, S. Tautz, D. Dini, A. Breidenassel, B. Galler, and S. Ltge, Appl. Phys. Lett. **95**, 051104 (2009).
17) C. D. Santi et al., Microelectron. Reliab. **54**, 2147 (2014).
18) S. Tomiya, T. Hino, S. Goto, M. Takeya, and M. Ikeda, IEEE J. Sel. Top. Quantum Electron. **10**, 1277 (2004).
19) S. Tomiya, S. Goto, M. Takeya, and M. Ikeda, Phys. Stat. Sol. (A) **200**, 139 (2003).
20) M. Rossetti, T. M. Smeeton, W. S. Tan, M. Kauer, S. E. Hooper, J. Heffernan, H. Xiu, and C. J. Humphrey, Appl. Phys. Lett. **92**, 151110 (2008).
21) T. Schoedl, U. T. Schwarza, V. Kümmler, M. Furitsch, A. Leber, A. Miler, A. Lell, and V. Härle, J. Appl. Phys. **97**, 123102 (2005).
22) M. Meneghni, M. D. Lago, N. Triellin, G. Mura, M. Vanzi, G. Menehgesso, and E. Zanoni, Microelectron. Reliab. **52**, 804 (2012).
23) P. Y. Wen et al., J. Phys. D: Applied Physics **48**, 415101 (2015).
24) P. Y. Wen et al., Semicond. Sci. Technol. **30**, 125015 (2015).
25) S. S. Sui, M. Y. Tang, Y. D. Yang, J. L. Xiao, Y. Du, and Y. Z. Huang, Photon. Res. **3**, 289 (2015).
26) J. Van Campenhout, P. Rojo-Romeo, D. Van Thourhout, C. Seassal, P. Regreny, L. Di Cioccio, F. Jean-Marc, and R. Baets, J. Lightwave Technol. **25**, 1543 (2007).
27) J. X. Liu et al., Opt. Express **27**, 25943 (2019).
28) Y. Mei, R. B. Xu, H. Xu, L. Y. Ying, Z. W. Zheng, B. P. Zhang, M. Li, and J. Zhang, Semicond. Sci. Technol. **33**, 015016 (2018).
29) J. L. Ma, W. Li, and X. B. Luo, J. Appl. Phys. **119**, 125702 (2016).
30) W. L. Liu and A. A. Balandin, J. Appl. Phys. **97**, 073710 (2005).